Title:

A New Analytical Model for Vertical Ground Heat Exchangers with Neumann and Robin Boundary Condition on Ground Surface

Author: Aiqiang Pan, Lin Lu*, You Tian

Department of Building Services Engineering, The Hong Kong Polytechnic University, Hong Kong, China

Abstract:

Ground surface boundary conditions are important for the modeling of both horizontal and vertical ground heat exchangers (GHE) in some cases. This paper developed a new analytical model, using a new integral transform method, for vertical GHE under three different (Dirichlet, Neumann, and Robin) boundary conditions. The new method is flexible in defining ground surface condition and gives straightforward expressions of vertical heat flux around vertical GHE. Using the newly developed and validated model, the effects of different types of ground surface boundary conditions on temperature responses of vertical GHE is studied theoretically. It is found that the effects would be limited in the dimensionless depth of about 200, so it would more important to employ the right ground surface boundary condition according to the specific cases for vertical GHE with shorter depth. Also, by defining a Robin boundary condition, the thermal impact can be, and for the first time, examined. Moreover, the case study demonstrated that when the borehole top is covered with insulation material, using Dirichlet boundary condition underestimated the borehole wall temperatures. Although the average difference of a single borehole may be only about 1 °C after 90 days of heat injection, the thermal energy storage of borehole groups in the long time can still be significant underestimated. The new model proposed in this paper can be widely used to offer more accurate temperature prediction of vertical borehole by defining the right boundary condition for the specific applications.

Keywords:

Vertical ground heat exchangers; Analytical model; Robin ground surface boundary conditions; Thermal impact on ground surface

Highlights:

1. a new integral transform method used to derive analytical models for vertical GHE
2. convenient to define different ground surface boundary conditions in analytical model
3. effects of different ground surface boundary conditions on vertical GHE were analyzed
4. Robin ground surface boundary condition is suggested for modeling in certain cases
5. thermal impact on ground surface by operation of vertical GHE is firstly analyzed

Nomenclature

z vertical axis in cylindrical coordinate

r radial axis in cylindrical coordinate

h depth of disk heat source

h_d depth of ground heat exchanger

r_0 radius of ground heat exchanger

Q_l line heat source

q_z vertical heat flux

T temperature

k thermal conductivity

ρ density

c thermal capacity

s Laplace variable

φ Hankel variable

h_c convective heat transfer coefficient

Superscript

' dimensional variable

$\bar{}$ Laplace transformed variable

$\tilde{}$ Hankel transformed variable

1. Introduction

1.1 Background

Ground coupled heat pump (GCHP) technology has been recognized as one of the key technologies to achieve low-energy buildings. GCHP systems utilize the ground as heat sink or source for space cooling or heating. Because of relatively higher heat capacity and stable temperature of the ground compared with the ambient air, ground coupled heat pumps can have higher energy efficiency compared with traditional air source heat pumps [1]. The key component in GCHP systems is the ground heat exchangers (GHE), through which heat is injected into or extracted from the ground. GHE can be buried horizontally in relatively shallow ground, usually several meters beneath the ground surface. GHE can also be installed vertically as borehole GHE, stretching down to the deeper ground. Another relatively new type of vertical GHE is Pile GHE or energy pile. The pipes are prefixed on concrete reinforcing cage before pouring concrete. Horizontal and vertical GHE may have different advantages over each other. While horizontal GHE would require larger land area and be more affected by temperature variation on the ground surface compared with vertical GHE, the initial cost of horizontal GHE is generally less than borehole GHE. For example, the borehole drilling cost is generally higher than the trenching cost of horizontal GHE.

The past decades have seen the extensive researches on both vertical and horizontal GHE. In 2010, Yang et al. [2] reviewed the various analytical models calculating the heat transfer process both inside and outside the boreholes. In 2012, Yuan et al. [3] summarized both analytical and the numerical models for borehole GHE. In 2014, Li et al. [4] compared the analytical models for vertical GHE in detail from the perspective of time and space scales. In 2017, Fadejev et al. [5] summarized the analytical and numerical models of pile GHE. They concluded that for the design of pile GHE, the existing software packages for the design of borehole GHE need to include the variable ground surface boundary condition. With regards to horizontal GHE, Cui et al. [6] conducted a comprehensive review of GCHP systems with

horizontal GHE in 2019. The existing analytical and numerical models of horizontal GHE were summarized in detail. The different ground surface conditions adopted by different researchers were listed in the cited paper [6]. The authors recommended that a more real ground surface boundary condition should be incorporated in modeling of horizontal GHE. In view of these researches, the state-of-art research on modeling the ground surface boundary conditions in both analytical and numerical models of GHE are further reviewed below.

1.2 Modeling the ground surface in horizontal GHE

Ground surface, as an upper boundary in modeling horizontal GHE, has significant effects on the thermal performance of horizontal GHE. To model this boundary effect, some researchers adopted a constant temperature [7] or time-varying temperature [8-10] to represent the ground surface boundary condition in numerical models. In analytical models, some researcher also adopted a time-varying temperature function [11, 12]. The time-varying temperature functions commonly take the form of an annual average temperature (either air or ground temperature) plus an amplitude function (usually a sinusoidal function). Such functions are called soil temperature harmonic function. Assigning only the temperature value on the ground surface is defining a Dirichlet boundary condition (first kind boundary condition). This simplification on ground surface condition was shown to have large error in modeling horizontal GHE [13].

As a Dirichlet boundary condition might fail to model a real ground surface boundary condition, researchers employed the energy balance equation to describe the heat exchange between ground surface and surface air in numerical models [14-20]. Using the energy balance equation, which is a Robin boundary condition (third kind boundary condition), is closer to a real ground surface condition and hence more accurate for the modeling of horizontal GHE. The specific expression of the energy balance equation may vary, but generally includes the conductive, convective, radiative

heat flux, and heat flux due to evaporation (latent heat transfer). Oosterkamp et al. [18] compared the accuracy of three different ground surface boundary conditions, i.e. measured air temperature, menasured soil surface temperature and surface energy balance equation. It was found that using the menasured soil surface temperature and surface energy balance equation as the ground surface boundary condition are accurate, while using the measured air temperature as the boundary condition is inaccurate. A similar conclusion was drawn by Bortoloni et al. [17]. They compared the results using three different boundary conditions (first, second, and third kind boundary conditions) in modeling horizontal GHE. It was concluded that employing the surface energy balance equation gives accurate results. Using the equivalent ground surface temperature obtained from energy balance equation may also yield acceptable results, while using the second kind boundary condition may result in noticeable error.

To summarize, for modeling horizontal GHE, the ground surface boundary condition should be carefully treated. Employing the changing air temperature on ground surface as a Dirichlet boundary condition on ground surface is generally not suggested. Accurate modeling requires in-site measurement of ground temperature or employing an energy balance equation as a Robin boundary condition to represent the ground surface. However, the Robin boundary condition is only implemented in numerical models at present, and the existing analytical models still employ a Dirichlet boundary condition in modeling horizontal GHE.

1.3 Modeling the ground surface in vertical GHE

The effect of ground surface on the thermal performance of vertical GHE is relatively less studied compared with horizontal GHE. The vertical temperature variation along borehole GHE caused by ground surface was considered by calculating an integral average temperature along the depth of borehole GHE, since using the temperature at the middle depth of borehole GHE is generally found to lead to overestimation [21]. The average temperature was then used in evaluating the thermal

response test (TRT) data to calculate the effective thermal conductivity and borehole thermal resistance.

In the last few years, the ground surface has drawn more attention in modeling vertical GHE. Bidarmaghz et al. [22] studied the effect of ground surface on the thermal performance of vertical GHE with numerical models. Their results suggested that the thermal impact of ground surface may lead to the reduction of effective GHE length. For a 30 m deep GHE, the effective length would be 11% less. For a 50 m deep GHE, the effective length would be 6% less.

In a study originally focusing on the vertical heat flux around borehole GHE, researchers found that the vertical heat flux around GHE may accelerate ground temperature recovery [23]. More importantly, they found that two thirds of shallow geothermal energy come from atmosphere, while one third comes from deep ground. This research raised the importance of the vertical heat flux through ground surface in modeling borehole GHE, which had not been carefully examined previously. Neglecting this vertical heat flux means that the geothermal energy obtained is from earth interior, which is not the real case. Another research also evaluated the effect of axial heat transfer in the ground on the energy efficiency of borehole GHE [24]. They concluded that the effect is considerable in the long term, and the heat transfer through the ground surface, including convection, solar radiation, and long-wave radiation, would affect the fluid temperature in the borehole. Therefore, the consideration of ground surface is important for long-term performance analysis of vertical GHE.

The changing ground surface temperature was considered in an analytical model to analyze its effects on thermal performance of borehole GHE by Rivera et al. [25]. It was found that different land surface conditions could have significant effects on the ground thermal condition. In the research, the different land surface conditions, considered as temperature boundary conditions, are Dirichlet boundary conditions. In later research, they adopted a Cauchy boundary condition to represent the ground surface boundary condition [26, 27]. The Cauchy boundary condition offers a better

modeling of the ground surface condition, as the convective heat transfer between soil and ambient on ground surface is considered. In the two cited papers, the Cauchy boundary condition considered is assumed to be homogeneous firstly, and then the surface air temperature (SAT) is considered as the ground surface temperature (GST) to relax the previous homogeneous assumption. The Cauchy boundary condition can be considered as a special version of Robin boundary condition that the temperature value and heat flux are both determined on the boundary. As the authors also specified [26], the Cauchy boundary condition is a simplified surrogate of a real boundary condition, which can be described by an energy balance equation as a Robin boundary condition.

In summary, the consideration of ground surface boundary condition is important for the utilization of shallow geothermal energy through both horizontal and vertical GHE. While in modeling horizontal GHE, the Robin boundary condition, which is closer to the real ground surface condition, has been commonly employed in numerical models, it has not been employed in modeling vertical GHE. The existing analytical models of vertical GHE always consider the ground surface as a Dirichlet or Cauchy boundary condition. Also, in last few years, researchers have reported the effect of the vertical heat flux on the long-term energy efficiency of vertical GHE and highlighted the importance of considering a real ground surface boundary condition in modeling vertical GHE.

Therefore, this paper aims to develop an analytical model for vertical GHE with a Robin ground surface boundary condition. The integral transform method is employed to develop the analytical model. This method is flexible in defining ground surface boundary condition and is also simple in form. Also, the vertical heat flux around vertical GHE can be easily calculated with explicit mathematical expressions. Using the developed model, the solution of temperature and vertical heat flux around vertical GHE under different types of boundary conditions are calculated and analyzed.

Furthermore, by defining a Robin ground surface boundary condition, this paper has newly studied the thermal impact (temperature and vertical heat flux) on the ground

surface caused by the operation of vertical GHE. In previous research, defining the Dirichlet ground surface boundary condition for vertical GHE means that the ground surface temperature, which is only the temperature without the operation of vertical GHE, would be exactly the temperature defined on ground surface. Such a definition just neglects the thermal impact of vertical GHE, since the ground temperatures with and without buried heat source would be different in real cases. This shortcoming is overcome by defining a Robin boundary condition on the ground surface, as in a Robin boundary condition, the temperature is not defined but a convective heat transfer coefficient.

2. Model development

2.1 Vertical heat flux

For the ground considered as a semi-infinite medium, the expressions representing three different boundary conditions on ground surface under cylindrical coordinate are:

$$T'(r',0,t')=f_T(t') \tag{1}$$

$$-k\left.\frac{\partial T'(r',z,t')}{\partial z'}\right|_{z=0}=f_q(t') \tag{2}$$

$$-k\left.\frac{\partial T'(r',z,t')}{\partial z'}\right|_{z=0}+h_c'T'(r',0,t')=f_q(t')+h_c'f_{T_a}(t') \tag{3}$$

The superscript ' denotes dimensional variables. z' is positive downward. $T'(r',0,t')$ is the ground surface temperature. $\left.-k\frac{\partial T'(r',z,t')}{\partial z'}\right|_{z=0}$ is the heat flux through ground surface. h_c is convective heat transfer coefficient on ground surface. $f_T(t')$ is the function representing the ground surface temperature and $f_{T_a}(t')$ is the function representing the air temperature on ground surface. Equation (1), (2), and (3) is the Dirichlet, Neumann, and Robin boundary condition respectively. For a homogeneous boundary condition of each type, $f_T(t')$ and $f_q(t')$ equal zero. For a nonhomogeneous boundary condition, $f_T(t')$ and $f_q(t')$ equal the specific value on the boundary.

Compared with the Dirichlet boundary condition, both the Neumann and Robin boundary conditions contain the vertical heat flux through the ground surface. The vertical heat flux around vertical GHE in the long term is also a research objective in this paper. Therefore, it would be convenient to incorporate the vertical heat flux, i.e. $q_z'(r',z',t')=-k\frac{\partial T'(r',z',t')}{\partial z'}$ into the model derivation.

The Fourier heat conduction equation under cylindrical coordinate is:

$$\rho c\frac{\partial T'}{\partial t'}=k\left(\frac{\partial^2 T'}{\partial r'^2}+\frac{1}{r'}\frac{\partial T'}{\partial r'}+\frac{\partial^2 T'}{\partial z'^2}\right) \tag{4}$$

With the definition of vertical heat flux, Equation (4) can be rewritten into two equations containing the vertical heat flux that govern the heat transfer process:

$$\begin{aligned}\frac{\partial T'}{\partial z'} &= -\frac{1}{k}q_z' \\ \frac{\partial q_z'}{\partial z'} &= k\left(\frac{\partial^2 T'}{\partial r'^2}+\frac{1}{r'}\frac{\partial T'}{\partial r'}\right)-\rho c\frac{\partial T'}{\partial t'}\end{aligned} \tag{5}$$

Also, vertical GHE, which are usually considered as line or cylindrical heat source [28], can also be represented with vertical heat flux. Considering vertical GHE as a cylindrical heat source, it can be decomposed into numerous disk heat sources overlapping along the depth of vertical GHE (Figure 1).

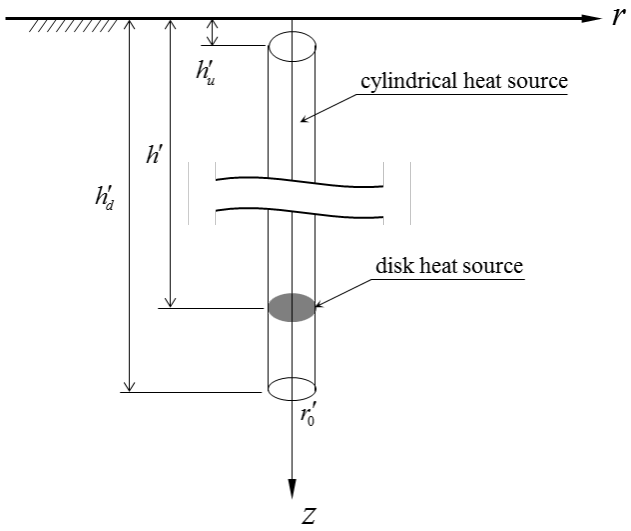

Figure 1 Cylindrical heat source composed by disk heat sources

Assuming the intensity of the cylindrical heat source is Q_l' (W/m), then the disk heat source expressed in the form of vertical heat flux is:

$$q_{z,s}' = \frac{Q_l' dh'}{\pi r_0'^2} \quad (r' \le r_0' \ ,\ h_u' \le h' \le h_d') \tag{6}$$

The solution of cylindrical heat source is obtained by integrating the solution of disk heat source along the depth of vertical GHE. The method of representing cylindrical heat source is validated by comparing with other analytical solutions of cylindrical heat source latter in this paper.

2.2 General solution

There are two assumptions concerning the ground in the model derivation. The two assumptions are common in deriving analytical models of vertical GHE. The first assumption is that the surrounding soil is homogeneous with constant thermal properties. The second is that the initial temperature of the ground is assumed to be uniform. The initial temperature distribution can be considered as internal heat source at initial time and the uniform assumption can be relaxed by superposition method [26].

By using the following dimensionless quantities:

$$r=\frac{r'}{r_0'}, z=\frac{z'}{r_0'}, h=\frac{h'}{r_0'}, h_u=\frac{h_u'}{r_0'}, h_d=\frac{h_d'}{r_0'}, t=\frac{kt'}{\rho c r_0'^2}, T=\frac{k(T'-T_0')}{Q_l'}, q_z=\frac{r_0' q_z'}{Q_l'}, h_c=\frac{r_0' h_c'}{k},$$

the dimensional governing equations and disk heat source can be nondimensionalized.

$$\begin{aligned}\frac{\partial T}{\partial z}&=-q_z\\ \frac{\partial q_z}{\partial z}&=\frac{\partial^2 T}{\partial r^2}+\frac{1}{r}\frac{\partial T}{\partial r}-\frac{\partial T}{\partial t}\end{aligned} \tag{7}$$

$$q_{z,s}=\frac{dh}{\pi} \quad (r\le 1,\ h_u\le h\le h_d) \tag{8}$$

Writing equations (7) in the matrix form gives:

$$\frac{\partial}{\partial z}X(r,z,t)=A(r,t)X(r,z,t) \tag{9}$$

where $X(r,z,t)=\begin{pmatrix}T(r,z,t)\\ q_z(r,z,t)\end{pmatrix}, A(r,t)=\begin{pmatrix}0 & -1\\ \frac{\partial^2}{\partial r^2}+\frac{1}{r}\frac{\partial}{\partial r}-\frac{\partial}{\partial t} & 0\end{pmatrix}.$

Applying the Laplace transform $L[F(t)]=\bar{F}(s)=\int_0^\infty e^{-st}F(t)dt$ on Equation (9) and utilizing the property of the Laplace transform $L[\frac{\partial}{\partial t}F(t)]=s\bar{F}(s)-F(+0)$, Equation (9) turns into

$$\frac{\partial}{\partial z}\bar{X}(r,z,s)=\bar{A}(r,s)\bar{X}(r,z,s) \tag{10}$$

where $\bar{A}(r,s)=\begin{pmatrix}0 & -1\\ \frac{\partial^2}{\partial r^2}+\frac{1}{r}\frac{\partial}{\partial r}-s & 0\end{pmatrix}.$

Then, apply the Hankel transform (0-order) $H[F(r)]=\overline{\overline{F}}(\varphi)=\int_0^\infty rJ_0(\varphi r)F(r)dr$ on Equation (10), it changes into

$$\frac{d}{dz}\overline{\overline{X}}(\varphi,z,s)=\overline{\overline{A}}(\varphi,s)\overline{\overline{X}}(\varphi,z,s) \tag{11}$$

where $J_0(x)$ is the 0-order Bessel function of first kind

$J_0(x)=\frac{1}{\pi}\int_0^\pi e^{ix\cos\theta}d\theta=\frac{1}{\pi}\int_0^\pi \cos(x\sin\theta)d\theta$, and $\overline{\overline{A}}(\varphi,s)=\begin{pmatrix}0 & -1\\ -\varphi^2-s & 0\end{pmatrix}$. In the Hankel transform operation, the following property of Hankel transform has been used [29]: for $\lim_{r\to\infty}F(r)=0$, $H[\frac{\partial^2F(r)}{\partial r^2}+\frac{1}{r}\frac{\partial F(r)}{\partial r}]=-\varphi^2H[F(r)]$.

Equation (11) is a first order ordinary differential equation. The general solution of it can be easily obtained:

$$\overline{\overline{X}}(\varphi,z,s)=B(\varphi,z,s)\overline{\overline{X}}(\varphi,0,s) \tag{12}$$

In Equation (12), $B(\varphi,z,s)=\exp[z\overline{\overline{A}}(\varphi,s)]$ is a coefficient matrix which can be calculated with $B(\varphi,z,s)=a_0I+a_1\overline{\overline{A}}$ according to Cayley-Hamilton theorem [30]. Solving the proper equation of $\overline{\overline{A}}(\varphi,s)$, the two eigenvalues of it can be obtained: $\gamma_{1,2}=\pm\sqrt{\varphi^2+s}$. Let $\gamma=\sqrt{\varphi^2+s}$, the coefficient a_0,a_1 can be obtained:

$$a_0=\frac{\exp(\gamma z)+\exp(-\gamma z)}{2} \tag{13}$$

$$a_1=\frac{\exp(\gamma z)-\exp(-\gamma z)}{2\gamma} \tag{14}$$

So that $B(\varphi,z,s)$ is determined. Also, in the general solution Equation (12), $\overline{\overline{X}}(\varphi,0,s)=\begin{pmatrix}\overline{\overline{T}}(\varphi,0,s)\\ \overline{\overline{q}}_z(\varphi,0,s)\end{pmatrix}$ is the ground surface boundary condition after Laplace and Hankel transform. This is the convenience of the integral transform method that the different boundary conditions can be easily assigned on the ground surface.

2.3 Solution for vertical GHE with different boundary conditions

At depth H which is deeper than the depth of disk heat source h, the solution of $\bar{\bar{X}}(\varphi, H, s)$ is:

$$\bar{\bar{X}}(\varphi, H, s) = B(\varphi, H, s)\bar{\bar{X}}(\varphi, 0, s) + B(\varphi, H, s)_{z=H-h}\begin{pmatrix} 0 \\ \dfrac{J_1(\varphi)dh}{\pi\varphi s} \end{pmatrix} \tag{15}$$

where $\dfrac{J_1(\varphi)dh}{\pi\varphi s}$ is the dimensionless disk heat source $\dfrac{dh}{\pi}$ after performing Laplace and Hankel transform. Equation (15) can be rewritten as:

$$\begin{pmatrix} \bar{\bar{T}}(\varphi, H, s) \\ \bar{\bar{q}}_z(\varphi, H, s) \end{pmatrix} = \begin{pmatrix} a_0 & -a_1 \\ a_1(-\varphi^2 - s) & a_0 \end{pmatrix}\begin{pmatrix} \bar{\bar{T}}(\varphi, 0, s) \\ \bar{\bar{q}}_z(\varphi, 0, s) \end{pmatrix} + \frac{J_1(\varphi)dh}{\pi\varphi s}\begin{pmatrix} -a_1 \\ a_0 \end{pmatrix}_{z=H-h} \tag{16}$$

At infinite, $\bar{\bar{T}}(\varphi, \infty, s) = 0, \bar{\bar{q}}_z(\varphi, \infty, s) = 0$. Let $H \to \infty$, the relation between $\bar{\bar{q}}_z(\varphi, 0, s) = -k\left.\dfrac{\partial \bar{\bar{T}}(\varphi, z, s)}{\partial z}\right|_{z=0}$ and $\bar{\bar{T}}(\varphi, 0, s)$ can be determined:

$$\bar{\bar{q}}_z(\varphi, 0, s) = \gamma\bar{\bar{T}}(\varphi, 0, s) - \exp(-\gamma h)\frac{J_1(\varphi)dh}{\pi\varphi s} \tag{17}$$

It can be seen from Equation (17) that the vertical heat flux $\bar{\bar{q}}_z(\varphi, 0, s)$ and temperature $\bar{\bar{T}}(\varphi, 0, s)$ on ground surface are affected by the existence of the underground heat source $\dfrac{J_1(\varphi)dh}{\pi\varphi s}$. This is just the thermal impact caused by the operation of vertical GHE that we want to study.

2.3.1 Solution under Dirichlet boundary condition

For the Dirichlet boundary condition, $\bar{\bar{T}}(\varphi, 0, s)$ is given on the ground surface by $\bar{\bar{f}}_T(s)$. At depth z that is shallower than the depth of a disk heat source h ($z < h$), the solution according to the general solution is:

$$\bar{\bar{T}}(\varphi, z, s) = \exp(-\gamma z)\bar{\bar{f}}_T(s) + \frac{\exp[\gamma(z-h)] - \exp[-\gamma(z+h)]}{2\gamma}\frac{J_1(\varphi)dh}{\pi\varphi s} \tag{18}$$

$$\bar{\bar{q}}_z(\varphi, z, s) = \gamma\exp(-\gamma z)\bar{\bar{f}}_T(s) - \frac{\exp[\gamma(z-h)] + \exp[-\gamma(z+h)]}{2}\frac{J_1(\varphi)dh}{\pi\varphi s} \tag{19}$$

At depth z that is deeper than the depth of a disk heat source h ($z > h$), the solution

is:

$$\bar{\bar{T}}(\varphi,z,s)=\exp(-\gamma z)\,\bar{\bar{f}}_T(s)+\frac{\exp[-\gamma(z-h)]-\exp[-\gamma(z+h)]}{2\gamma}\frac{J_1(\varphi)dh}{\pi\varphi s} \tag{20}$$

$$\bar{\bar{q}}_z(\varphi,z,s)=\gamma\exp(-\gamma z)\,\bar{\bar{f}}_T(s)+\frac{\exp[-\gamma(z-h)]-\exp[-\gamma(z+h)]}{2}\frac{J_1(\varphi)dh}{\pi\varphi s} \tag{21}$$

Equations (18) to (21) are the solutions of the disk heat source. The solutions of cylindrical heat source, i.e., vertical GHE, can be obtained by integrating the solution of the disk heat source along the depth of GHE (h_u to h_d), which gives:

$$\bar{\bar{T}}(\varphi,z,s)=\exp(-\gamma z)\,\bar{\bar{f}}_T(s)+[1-\exp(-\gamma z)\,a_0\big|_{z=h_u}-\gamma\exp(-\gamma h_d)a_1]\frac{J_1(\varphi)}{\pi\varphi s\gamma^2} \tag{22}$$

$$\bar{\bar{q}}_z(\varphi,z,s)=\gamma\exp(-\gamma z)\,\bar{\bar{f}}_T(s)+\left[-\exp(-\gamma z)\,a_0\big|_{z=h_u}+\exp(-\gamma h_d)a_0\right]\frac{J_1(\varphi)}{\pi\varphi s\gamma} \tag{23}$$

2.3.2 Solution under Neumann boundary condition

For the Neumann boundary condition, only $\bar{\bar{q}}_z(\varphi,0,s)$ is given on the ground surface by $\bar{\bar{f}}_q(s)$. At depth z that is shallower than the depth of a disk heat source h ($z<h$), the solution according to the general solution is:

$$\bar{\bar{T}}(\varphi,z,s)=\frac{\exp(-\gamma z)}{\gamma}\,\bar{\bar{f}}_q(s)+\frac{\exp[\gamma(z-h)]+\exp[-\gamma(z+h)]}{2\gamma}\frac{J_1(\varphi)dh}{\pi\varphi s} \tag{24}$$

$$\bar{\bar{q}}_z(\varphi,z,s)=\exp(-\gamma z)\,\bar{\bar{f}}_q(s)-\frac{\exp[\gamma(z-h)]-\exp[-\gamma(z+h)]}{2}\frac{J_1(\varphi)dh}{\pi\varphi s} \tag{25}$$

At depth z that is deeper than the depth of a disk heat source h ($z>h$), the solution is:

$$\bar{\bar{T}}(\varphi,z,s)=\frac{\exp(-\gamma z)}{\gamma}\,\bar{\bar{f}}_q(s)+\frac{\exp[-\gamma(z-h)]+\exp[-\gamma(z+h)]}{2\gamma}\frac{J_1(\varphi)dh}{\pi\varphi s} \tag{26}$$

$$\bar{\bar{q}}_z(\varphi,z,s)=\exp(-\gamma z)\,\bar{\bar{f}}_q(s)+\frac{\exp[-\gamma(z-h)]+\exp[-\gamma(z+h)]}{2}\frac{J_1(\varphi)dh}{\pi\varphi s} \tag{27}$$

Equations (24) to (27) are the solutions of the disk heat source. Integrating the solution of the disk heat source along the depth of GHE (h_u to h_d) gives the solution of vertical GHE:

$$\bar{\bar{T}}(\varphi,z,s)=\frac{\exp(-\gamma z)}{\gamma}\,\bar{\bar{f}}_q(s)+\left[1-\gamma\exp(-\gamma z)\,a_1\big|_{h_u}-\exp(-\gamma h_d)a_0\right]\frac{J_1(\varphi)}{\pi\varphi s\gamma^2} \tag{28}$$

$$\bar{\bar{q}}_z(\varphi,z,s)=\exp(-\gamma z)\,\bar{\bar{f}}_q(s)+\left[-\exp(-\gamma z)\,a_1\big|_{h_u}+\exp(-\gamma h_d)a_1\right]\frac{J_1(\varphi)}{\pi\varphi s} \tag{29}$$

2.3.3 Solution under Robin boundary condition

For the Robin boundary condition, instead of giving $\bar{\bar{T}}(\varphi,0,s)$ or $\bar{\bar{q}}_z(\varphi,0,s)$ on the ground surface, only their relationship is defined according to Robin boundary condition that $\bar{\bar{q}}_z(\varphi,0,s)+h_c\bar{\bar{T}}(\varphi,0,s)=\bar{\bar{f}}_q(s)+h_c\bar{\bar{f}}_{T_a}(s)$. With Equation (17), the expressions of $\bar{\bar{T}}(\varphi,0,s)$ or $\bar{\bar{q}}_z(\varphi,0,s)$ can be obtained:

$$\bar{\bar{T}}(\varphi,0,s)=\frac{\bar{\bar{f}}_q(s)+h_c\bar{\bar{f}}_{T_a}(s)}{\gamma+h_c}+\frac{\exp(-\gamma h)}{\gamma+h_c}\frac{J_1(\varphi)dh}{\pi\varphi s} \tag{30}$$

$$\bar{\bar{q}}_z(\varphi,0,s)=\frac{\gamma}{\gamma+h_c}\left[\bar{\bar{f}}_q(s)+h_c\bar{\bar{f}}_{T_a}(s)\right]-\frac{h_c}{\gamma+h_c}\exp(-\gamma h)\frac{J_1(\varphi)dh}{\pi\varphi s} \tag{31}$$

At depth z that is shallower than the depth of a disk heat source h ($z<h$), the solution according to the general solution is:

$$\begin{aligned}\bar{\bar{T}}(\varphi,z,s)&=\frac{\exp(-\gamma z)}{\gamma+h_c}\left[\bar{\bar{f}}_q(s)+h_c\bar{\bar{f}}_{T_a}(s)\right]\\&+\left[\frac{\exp[\gamma(z-h)]}{2\gamma}+\frac{(\gamma-h_c)\exp[-\gamma(z+h)]}{2\gamma(\gamma+h_c)}\right]\frac{J_1(\varphi)dh}{\pi\varphi s}\end{aligned} \tag{32}$$

$$\begin{aligned}\bar{\bar{q}}_z(\varphi,z,s)&=\frac{\gamma\exp(-\gamma z)}{\gamma+h_c}\left[\bar{\bar{f}}_q(s)+h_c\bar{\bar{f}}_{T_a}(s)\right]\\&+\left[\frac{-\exp[\gamma(z-h)]}{2}+\frac{(\gamma-h_c)\exp[-\gamma(z+h)]}{2(\gamma+h_c)}\right]\frac{J_1(\varphi)dh}{\pi\varphi s}\end{aligned} \tag{33}$$

At depth z that is deeper than the depth of a disk heat source h ($z>h$), the solution is:

$$\begin{aligned}\bar{\bar{T}}(\varphi,z,s)&=\frac{\exp(-\gamma z)}{\gamma+h_c}\left[\bar{\bar{f}}_q(s)+h_c\bar{\bar{f}}_{T_a}(s)\right]\\&+\left[\frac{\exp[-\gamma(z-h)]}{2\gamma}+\frac{(\gamma-h_c)\exp[-\gamma(z+h)]}{2\gamma(\gamma+h_c)}\right]\frac{J_1(\varphi)dh}{\pi\varphi s}\end{aligned} \tag{34}$$

$$\begin{aligned}\bar{\bar{q}}_z(\varphi,z,s)&=\frac{\gamma\exp(-\gamma z)}{\gamma+h_c}\left[\bar{\bar{f}}_q(s)+h_c\bar{\bar{f}}_{T_a}(s)\right]\\&+\left[\frac{\exp[-\gamma(z-h)]}{2}+\frac{(\gamma-h_c)\exp[-\gamma(z+h)]}{2(\gamma+h_c)}\right]\frac{J_1(\varphi)dh}{\pi\varphi s}\end{aligned} \tag{35}$$

Equations (32) to (35) are the solutions of the disk heat source. Integrating the solution of the disk heat source along the depth of GHE (h_u to h_d) gives the solution

of vertical GHE:

$$T(\varphi,z,s)=\frac{\exp(-\gamma z)}{\gamma+h_c}\left[\,\overline{\overline{f}}_q(s)+h_c\,\overline{\overline{f}}_{T_a}(s)\right]+\left[\begin{array}{l}\dfrac{2-\exp[-\gamma(z-h_u)]-\exp[\gamma(z-h_d)]}{2\gamma^2}\\+\dfrac{(\gamma-h_c)\exp(-\gamma z)\left[\exp(-\gamma h_u)-\exp(-\gamma h_d)\right]}{2\gamma^2(\gamma+h_c)}\end{array}\right]\frac{J_1(\varphi)}{\pi\varphi s} \tag{36}$$

$$\overline{\overline{q}}_z(\varphi,z,s)=\frac{\gamma\exp(-\gamma z)}{\gamma+h_c}\left[\,\overline{\overline{f}}_q(s)+h_c\,\overline{\overline{f}}_{T_a}(s)\right]+\left[\begin{array}{l}\dfrac{-\exp[-\gamma(z-h_u)]+\exp[\gamma(z-h_d)]}{2\gamma}\\+\dfrac{(\gamma-h_c)\exp(-\gamma z)\left[\exp(-\gamma h_u)-\exp(-\gamma h_d)\right]}{2\gamma(\gamma+h_c)}\end{array}\right]\frac{J_1(\varphi)}{\pi\varphi s} \tag{37}$$

2.4 Implementing different boundary conditions

The analytical solutions for vertical GHE with different boundary conditions have been derived above. The solution equations are further summarized in Table 1.

Table 1 Analytical solutions with different boundary conditions

boundary conditions	Solution Equations	
	Temperature	Heat flux
Dirichlet type: $T(r,0,t)=f_T(t)$	(22)	(23)
Neumann type: $q_z(r,0,t)=f_q(t)$	(28)	(29)
Robin type: $q_z(r,0,t)+h_cT(r,0,t)=f_q(t)+h_c f_{T_a}(r,0,t)$	(36)	(37)

The six solution equations listed in Table 1 under each boundary condition are a linear combination of two terms. One term contains the corresponding boundary condition as shown in Table 1. The other term contains the heat source $\frac{J_1(\varphi)}{\pi\varphi s}$. While the terms containing the corresponding boundary condition account for the contribution of the inhomogeneous boundary condition, the terms containing the heat source are the

solution under homogeneous boundary condition of each type. Letting $\overline{\overline{f}}_T(s)$ in Equations (22) and (23) equal zero, the equations give the solutions under fixed temperature boundary condition, where the fixed value is equal to the uniform initial temperature of the ground. Letting $\overline{\overline{f}}_q(s)$ in Equations (28) and (29) equal zero, the equations give the solutions under adiabatic boundary condition. And letting $\overline{\overline{f}}_q(s)+h_c\overline{\overline{f}}_{T_a}(s)$ in Equation (36) and (37) equal zero, the equation give the solutions under convective boundary condition. Clearly, the expressions of solutions under different homogenous boundary conditions are different.

Most of the existing analytical models for both horizontal and vertical GHE adopted a Dirichlet boundary condition. The ground surface is considered as a boundary with a given temperature $T(r,0,t)$. The given temperature might be the measured ground surface air temperature or the ground surface temperature. The Neumann boundary condition, i.e., giving the heat flux, is rarely used in modeling GHE.

In the Robin boundary condition, instead of giving the temperature $T(r,0,t)$ or heat flux $q_z(r,0,t)$ on the ground surface, the ground surface is described by an energy balance equation. As mentioned before, the energy balance equation generally includes conductive heat flux, convective, radiative, and latent heat flux. These heat fluxes are briefly presented in Table 2. The conductive heat flux is a term in the Robin boundary condition as shown in Table 1. The net radiative heat flux includes absorbed solar radiation (positive), incident long wave radiation (positive), and emitted long wave radiation (negative) [14, 19]. The convective heat flux is also called sensible heat flux [17, 18]. $T_a(r,0,t)$ is the temperature of ambient air on ground surface. The expression for latent heat flux takes different forms in the cited four papers. The energy balance equation described by the four terms are:

$$q_z(r,0,t)=q_{z,radi}(r,0,t)+q_{z,conv}(r,0,t)+q_{z,lat}(r,0,t) \tag{38}$$

Therefore, the expression for Robin boundary condition $q_z(r,0,t)+h_cT(r,0,t)$ would be:

$$q_z(r,0,t)+h_cT(r,0,t)=q_{z,radi}(r,0,t)+h_cT_a(r,0,t)+q_{z,lat}(r,0,t) \tag{39}$$

Table 2 Terms in energy balance equation

Terms in energy balance equation	
conductive heat flux $q_z(r,0,t)$	$-k\left.\frac{\partial T(r,z,t)}{\partial z}\right\|_{z=0}$
net radiative heat flux $q_{z,radi}(r,0,t)$	absorbed solar radiation incident/emitted long wave radiation
convective heat flux $q_{z,conv}(r,0,t)$	$h_c\left[T_a(r,0,t)-T(r,0,t)\right]$
latent heat flux $q_{z,lat}(r,0,t)$	---

From the theoretical point of view, using the measured undisturbed (without buried heat source) ground surface air temperature or the ground surface temperature as the Dirichlet-type ground surface boundary condition is not accurate for cases when there are buried heat source. Because it neglects the thermal effect of buried heat source on the boundary as shown in Equation (17). In view of this, one obvious advantage of using a Robin boundary condition is that ground surface temperature is not specified. But, the thermal effect of vertical GHE on the ground surface can be evaluated, which is an environmental point that previous research has generally neglected.

3. Model validation

The solution equations given in Table 1 contain the Laplace and Hankel variables. To get solutions in physical domain, these equations need to be converted from the transformed domain to physical domain. Although it is difficult to find the analytical inversion expressions of these equations, the numerical inversion can be an effective tool. The numerical inverse Hankel transform was performed using the mathematical toolbox released by EPFL [31], and the numerical inverse Laplace transform was performed using the algorithm by Valsa and Brancik [32]. Both of the algorithms have been proved to be effective and reasonably accurate for solving even more complex linear systems.

Also, to test the algorithm independence of numerical inversions, another numerical inverse Hankel transform by Baddour and Chouinard [33] and two other numerical Laplace transform methods (Abate and Whitt [34], and Villinger [35]) were also employed. The results by employing any combination of the inverse Hankel and Laplace transform methods were found to be the same.

Although the cylindrical heat source model for vertical GHE was developed through rigorous mathematical derivation, validation is still necessary for the model developed with a new method. The existing “solid” cylindrical heat source model for vertical GHE by Man et al. [28] can be a good reference model. The “solid” cylindrical heat source assumed a Dirichlet boundary condition with fixed temperature on ground surface. Therefore, as an validation example, the solution under Dirichlet boundary condition (Equation (22)) was compared with the existing “solid” cylindrical heat source model.

The temperature value of the point located at middle depth of vertical GHE on borehole surface ($r=1,\ z/h_d=0.5$) was compared. The comparison results are shown in Figure 2. The dimensionless temperature responses of the two models were compared at the dimensionless time ranging from 0.1 to 10000 for vertical GHE with three different dimensionless depths ($h_d=20,50,100$). It can be seen that the results

calculated by the new cylindrical model agree reasonably well with those of the “solid” cylindrical model. The dimensionless temperature responses at middle depth of the two models are almost the same and the values stabilize at 0.39, 0.53, 0.64 for vertical GHE with dimensionless depth of 20, 50, 100 respectively.

Also, the dimensionless temperature responses along the depth of vertical GHE ($r = 1,\ h_d = 20$) at the dimensionless time ranging from 0.1 to 10000 were compared (Figure 3). The maximum temperature generally located at the middle depth of GHE, but the maximum value location tends to move downwards as time advances. This is related with the fixed zero temperature boundary condition, as a Dirichlet boundary condition, on the ground surface. It can be explained by the vertical heat flux around vertical GHE that more heat flux would dissipate through the ground surface in the long term.

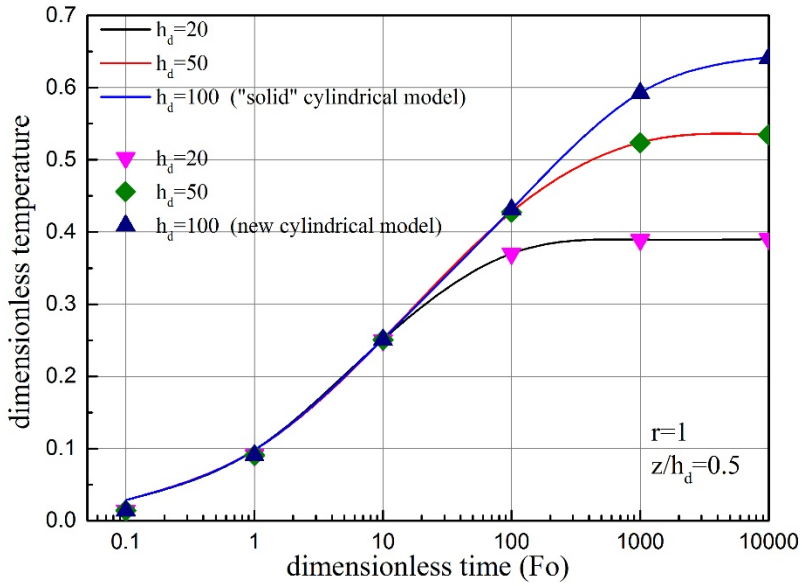

Figure 2 Comparison of temp. at the middle depth of vertical GHE

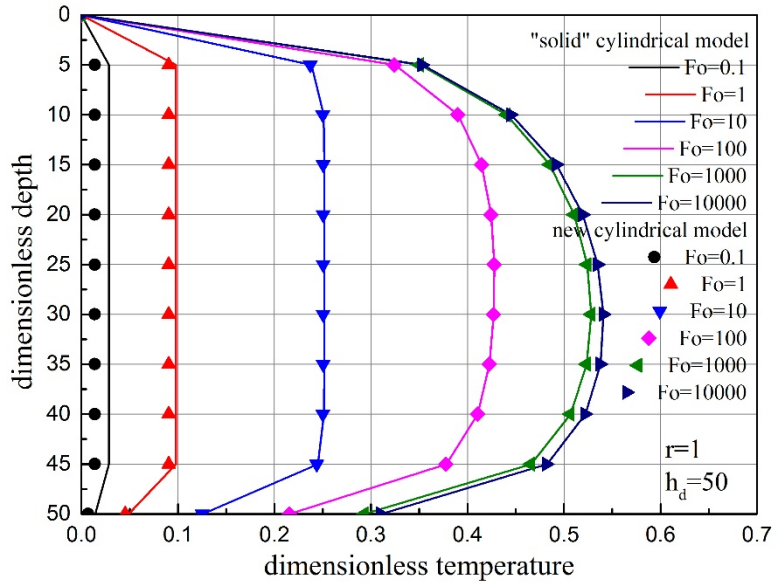

Figure 3 Comparison of temp. along the depth of PGHE

It has to be pointed out that at the very initial stage (small dimensionless time), the dimensionless temperature response of the new cylindrical model is smaller than the results of the “solid” cylindrical model. On one hand, the authors that proposed the “solid” cylindrical heat source model also pointed out that there is relatively large error between the analytical results and the numerical results at this very initial stage. On the other hand, the assumption concerning the heat source as mentioned above in the new cylindrical model may also be responsible for this difference. In the “solid” cylindrical heat source model, heat is assumed to be released from the cylindrical surface of the vertical GHE, whereas in the new cylindrical heat source model, heat is uniformly distributed in the solid cylindrical body. However, this temperature difference only exits at the very initial stage. In this study, the research focuses are the temperature and vertical heat flux under different ground surface boundary conditions, especially in the long term. Such a difference can be considered as a defect of the new model. But the model is predominant in considering different ground surface boundary conditions and calculating the vertical heat flux.

4. Results and Discussion

Using the new model, not only temperature, but also vertical heat flux around vertical GHE under different types of ground surface boundary conditions can be calculated. Since the inhomogeneous part of each boundary condition (the temperature variation on ground surface as the Dirichlet boundary condition, the vertical heat flux on ground surface as the Neumann boundary condition, and the energy balance equation on ground surface as the Robin boundary condition) always differ significantly with different specific locations and different climatic regions, only the homogeneous part of the three different types of boundary condition were calculated. So that the effect of choosing different ground surface boundary conditions in modeling vertical GHE can be compared excluding the disturbance of the specific inhomogeneous part of the three different boundary conditions to provide a theoretical and referential analysis.

Besides, the temperature and vertical heat flux on the ground surface under different ground surface boundaries were also calculated to discuss the thermal impact on the ground surface caused by the operation of vertical GHE as an environmental concern.

4.1 Temperature profile under different boundary conditions

4.1.1 Vertical GHE with different depths

Figure 4, Figure 5, and Figure 6 give the dimensionless temperature profile of vertical GHE with three different dimensionless depths (100, 200, and 500) under the three different ground surface boundary conditions. Clearly, for vertical GHE with different depths under different boundary conditions, the influence of ground surface affects deeper part of vertical GHE as dimensionless time gets larger.

Comparing the Dirichlet and Neumann boundary conditions (blue line for Dirichlet boundary condition and red line for Neumann boundary condition), at dimensionless time of 10000, the temperature difference covers the whole range of vertical GHE with dimensionless depths of 100 and 200. When the depth gets larger,

the difference seems to be limited in the dimensionless depth of 200, as can be seen from the temperature profile of the vertical GHE with a dimensionless depth of 500.

The temperature profiles under Robin boundary condition is marked with black line in the three figures. At each dimensionless time, the black lines are between the blue lines and red lines. For the homogeneous Dirichlet boundary condition, the temperature at ground surface is fixed at zero. For the homogeneous Neumann boundary condition, the temperature at ground surface has the largest value. In contrast, under the homogenous Robin boundary condition, the temperature at ground surface is between zero and the largest value. However, the temperature tends to stabilize at a certain value as can be seen that there is little increase in the temperature at ground surface when dimensionless time increases from 1000 to 10000. The stable value on ground surface is determined by the convective heat transfer coefficient.

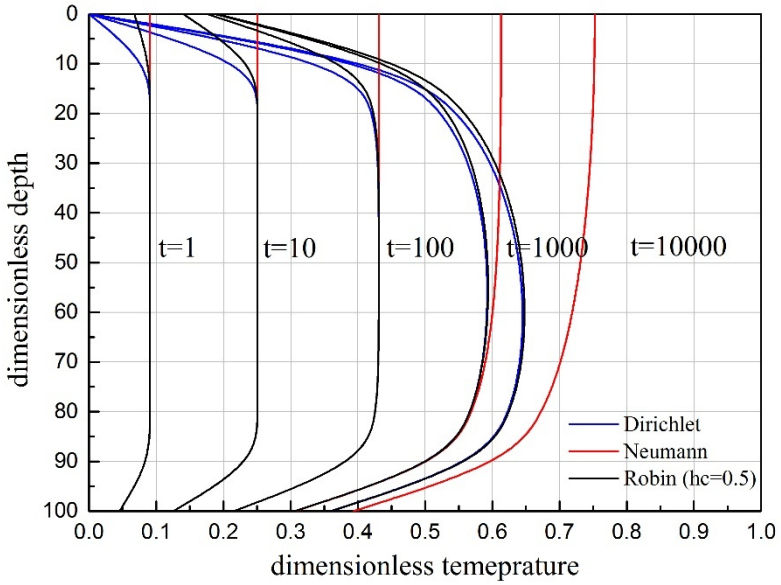

Figure 4 Temperature profile under different boundary conditions (dimensionless depth 100)

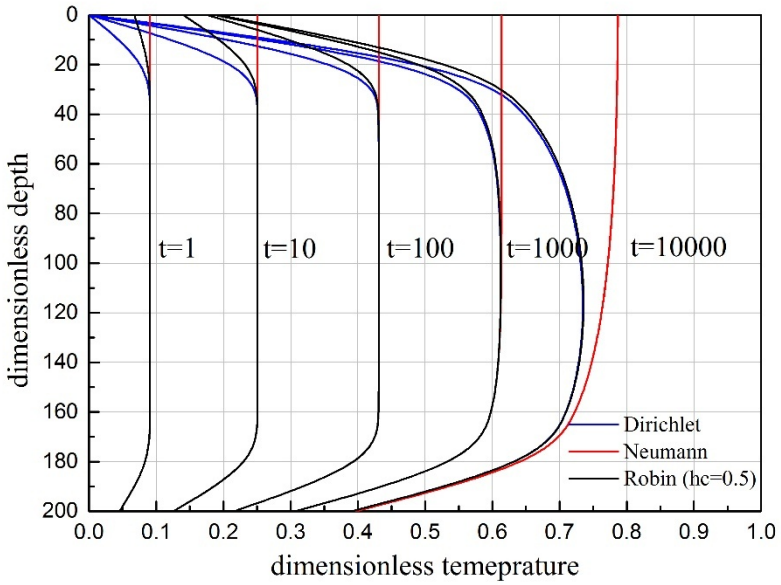

Figure 5 Temperature profile under different boundary conditions (dimensionless depth 200)

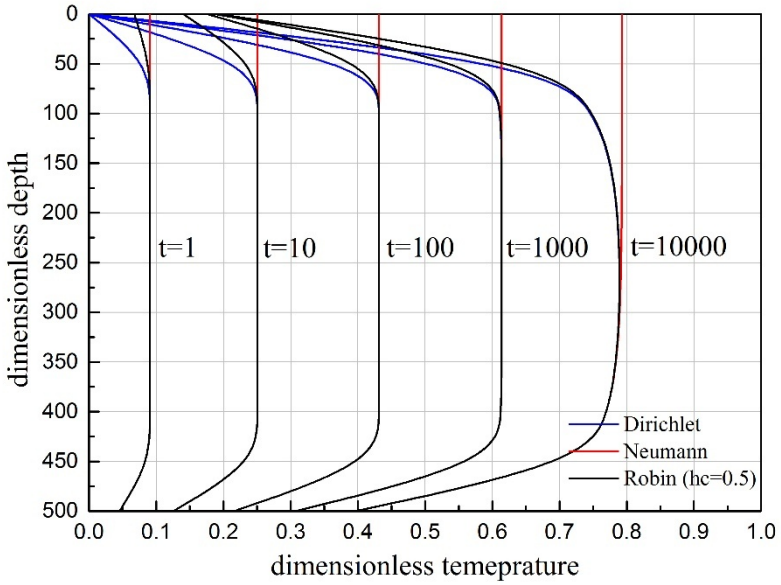

Figure 6 Temperature profile under different boundary conditions (dimensionless depth 500)

4.1.2 Robin boundary condition with different values of convective heat transfer coefficient

The temperature profile under Robin boundary condition would locate between the temperature profiles under Dirichlet and Neumann boundary condition. The specific location would be determined by the convective heat transfer coefficient on the ground surface. In the analysis above, its value is chosen to be 0.5 as an ordinary value for ground surface. For different practical environmental or man-made conditions on ground surface in different applications, the value might differ greatly [6, 27]. The

temperature profiles under three different values (0.1, 0.5 and 2.5) of convective heat transfer coefficient are shown in Figure 7. Smaller value of the convective heat transfer coefficient would close the temperature profile to the profile under Neumann boundary condition, while larger value would close the temperature to the profile under Dirichlet boundary condition. For the ground surface has a convective heat transfer coefficient of 0.1, 0.5, and 2.5, the dimensionless temperature on ground surface would stabilize at approximately 0.1, 0.2, and 0.4 respectively.

There is noticeable difference in temperature in the upper part of vertical GHE between Dirichlet boundary condition and Robin boundary condition with different heat transfer coefficients. Therefore, it is obvious that for vertical GHE with shorter depth, accurate modeling of ground surface boundary condition is more important. Also, the choice of ground surface boundary condition should be seriously considered for different applications. For example, for the application of borehole thermal energy storage (BTES) when the top ground is covered with insulation material, a smaller value of convective heat transfer coefficient might offer more accurate temperature profile along the top part of the boreholes. In the latter analysis, the value of convective heat transfer coefficient is set to vary widely to further study its effect on the thermal impact on ground surface caused by vertical GHE.

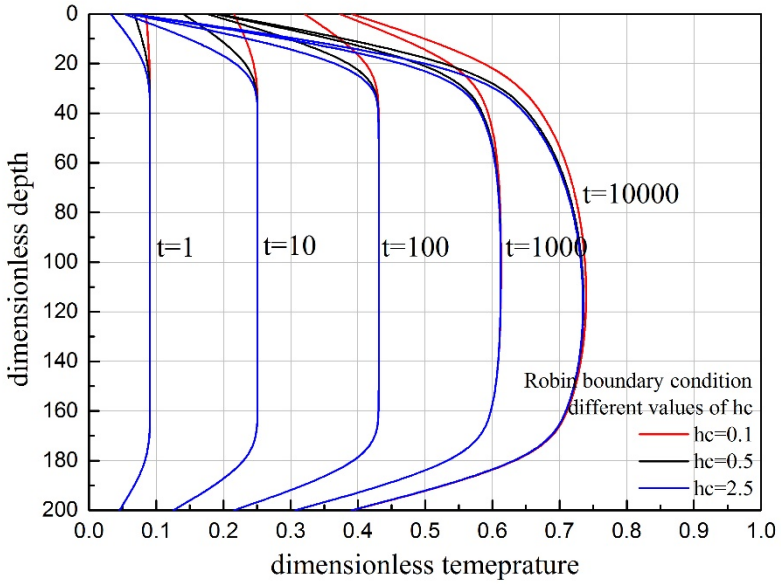

Figure 7 Temperature profile under Robin boundary condition with different values of h_c

4.2 Vertical heat flux

As a feature of the newly developed model, the vertical heat flux around vertical GHE can also be calculated with explicit mathematical expressions. The vertical heat flux at three different depths around vertical GHE (ground surface, middle depth, and bottom) under the three different ground surface boundary conditions are shown in Figure 8, Figure 9, and Figure 10. The dimensionless depth of the vertical GHE is 200. The dimensionless time is 10000. The vertical flux is positive when it is downward and negative when it is upward. The blue line stands for the vertical heat flux at GHE bottom, the black line stands for the vertical heat flux at middle depth, and the red line represents the vertical heat flux at ground surface.

Comparing the vertical heat flux under the three boundary conditions, it can be seen that the vertical heat flux at the bottom are the same, which implies that the boundary condition would not affect the transfer at the bottom of vertical GHE with dimensionless depth of 200. Also, the vertical heat fluxes at middle depth are always nearly zero, meaning that heat transfer around the middle depth is almost radial. In contrast, the vertical heat flux on ground surface differs greatly under the three different boundary conditions. Under Dirichlet boundary condition, the vertical heat flux is the largest, while under Neumann boundary condition, it is zero, since the homogeneous Neumann boundary condition is just an adiabatic boundary condition. The vertical heat flux under Robin boundary condition is smaller than that under Dirichlet boundary condition.

Under Dirichlet and Robin boundary condition, the vertical heat fluxes around GHE diminish quickly with radius. Within the dimensionless radius of 10, the value of vertical heat flux decreases to only about 90% of that at dimensionless radius of 1. At dimensionless radius larger than 30, the vertical heat flux is minimal, indicating that the vertical heat flux around vertical GHE on ground surface is limited in a circle with a radius of a few meters only.

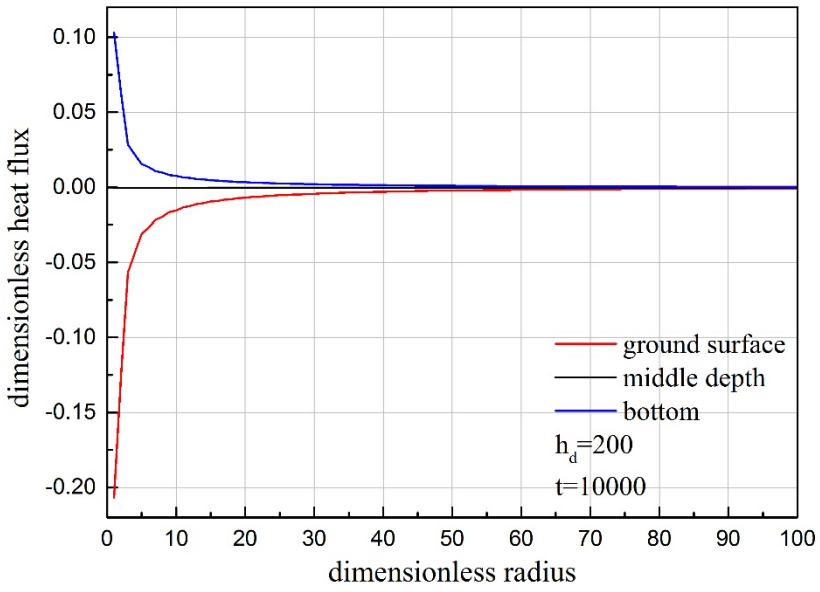

Figure 8 Vertical heat flux under Dirichlet boundary condition

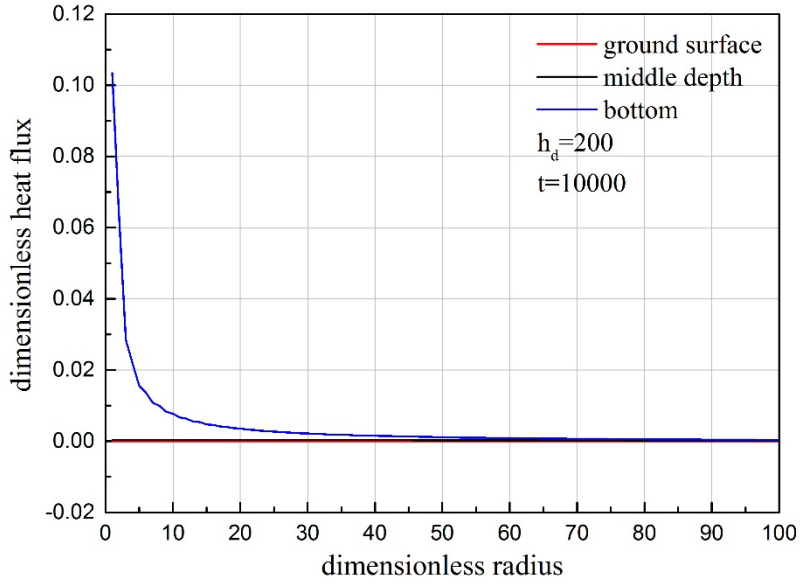

Figure 9 Vertical heat flux under Neumann boundary condition

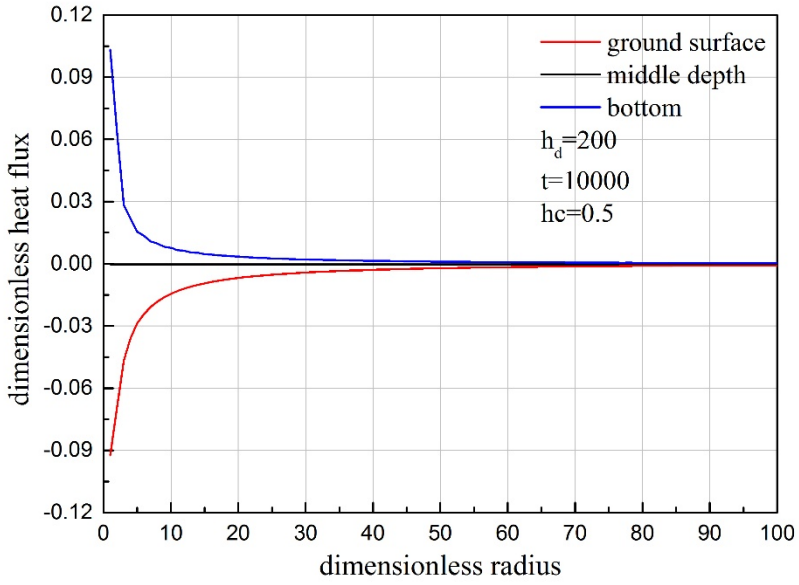

Figure 10 Vertical heat flux under Robin boundary condition

In Figure 10, the convective heat transfer coefficient on ground surface is 0.5. Similar to the analysis of temperature profile under different values of convective heat transfer coefficient, the vertical heat flux on ground surface under different values are plotted in Figure 11. When the value gets larger, the vertical heat flux gets larger, approaching to that under Dirichlet boundary condition. When the value gets smaller, the vertical heat flux gets smaller, approaching to that under Neumann boundary condition. The vertical heat flux drops dramatically with radius, and most of it is within the dimensionless radius of 10.

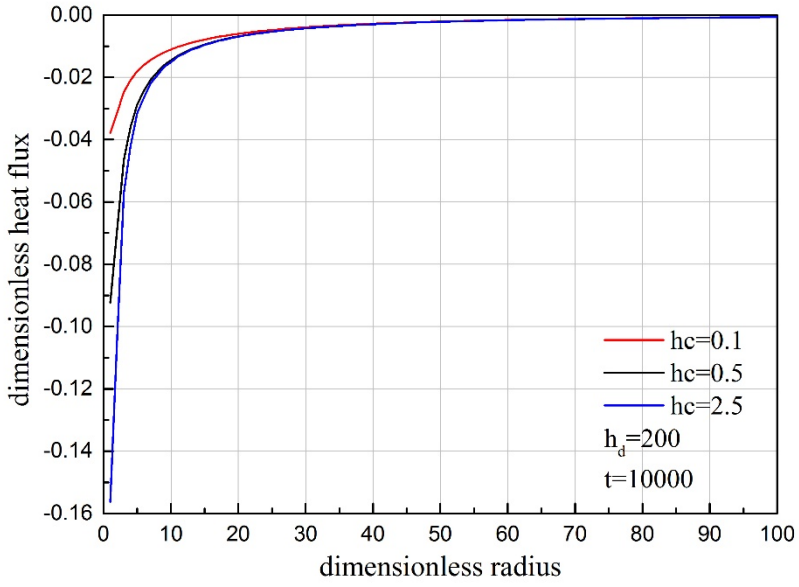

Figure 11 Vertical heat flux under Robin boundary condition with different h_c

4.3 Thermal impact of vertical GHE on ground surface

As discussed earlier, defining a Dirichlet or Neumann boundary condition on ground surface, which is the temperature or heat flux value without the existence of the buried heat source, cannot reveal the thermal impact on ground surface caused by the operation of vertical GHE. Instead, the temperature or heat flux on ground surface is not directly assigned in a Robin boundary condition, but rather the convective heat transfer coefficient on ground surface is defined. So that the temperature change and vertical heat flux on ground surface caused by the operation of vertical GHE can be calculated.

Using the newly developed model, the temperature and vertical heat flux on ground surface at different radiuses caused by the operation of vertical GHE were calculated (Figure 12, and Figure 13). The dimensionless convective heat transfer coefficient is set to range from 0.1 to 5, so that its effects on temperature and vertical heat flux can be analyzed.

In Figure 12, the dimensionless temperature decreases rapidly with the increase of convective heat transfer coefficient. When convective heat transfer coefficient increases from 0.1 to 1, the dimensionless temperature decreases from 0.39 to 0.12 at the dimensionless radius of 1. Also, the temperature decreases in radial direction. When the dimensionless convective heat transfer coefficient is 0.5, the temperature at radius 1 is 0.19, and it decreases quickly to 0.06 at radius of 5, and 0.03 at radius of 10.

In Figure 13, the dimensionless vertical heat flux declines more rapidly in radial direction compared with the temperature. At dimensionless radius larger than 5, the values of vertical heat flux are all below -0.04. Within the limited radius range (less than 5), the vertical heat flux (absolute value) increases with the increase of convective heat transfer coefficient, approaching a value of -0.18. This trend is opposite to that of temperature, since larger convective heat transfer coefficient means larger heat exchange on ground surface. Out of the limited radius range, the vertical heat flux

barely increases.

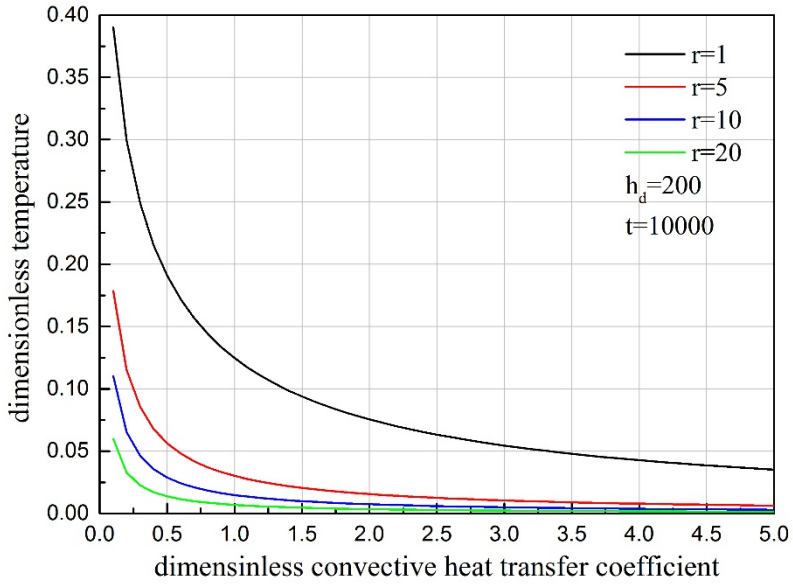

Figure 12 Temperature on ground surface with changing h_c

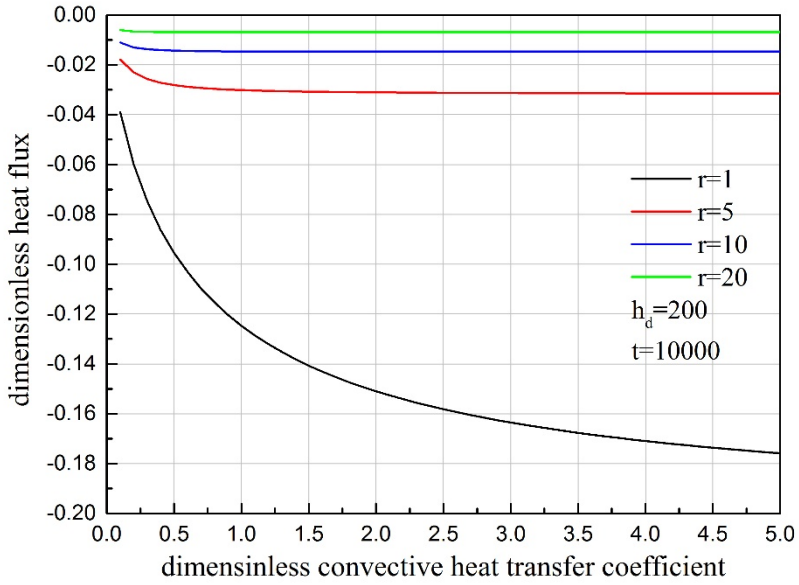

Figure 13 Vertical heat flux on ground surface with changing h_c

5. Case Study

In the application of soil borehole thermal energy storage systems, the depth of boreholes may be relatively small, and the top of boreholes is always covered with insulation material [36, 37]. The thermal conductivity of the insulation material is generally around 0.02 $W/(m\cdot K)$ whereas the thermal conductivity of the ground is generally around 2 $W/(m\cdot K)$. This insulation layer would prevent the loss of the heat stored in the ground through ground surface. In this case, the commonly employed Dirichlet boundary condition on ground surface would be inaccurate in predicting the borehole temperature responses. Instead, it is more reasonable to consider the top boundary condition as an insulated boundary condition, which is the homogeneous Neumann boundary condition, or more accurately, specify the heat transfer coefficient on the insulation layer, which would be a Robin boundary condition.

Therefore, a case study was conducted to show the effects of different ground surface boundary conditions on the borehole temperature responses using the new model in this paper. The parameters values used in the case study are given in Table 3. The insulation layer is treated in two ways in case study. One is that the insulation layer is assumed to provide perfect insulation, which that means the mean would all be trapped in the ground. The other is that the specific thermal resistance of insulation layer is considered, increasing the thermal transfer resistance between the ground and the above ambient air.

Table 3 Parameters in case study

Parameters	values
borehole upper depth h_u'	1 m
borehole bottom depth h_d'	15 m
borehole radius r_0'	0.05 m
ground thermal conductivity k	2 $W/(m\cdot K)$

ground soil density ρ	2000 kg/m^3
ground thermal capacity c	800 $J/(kg \cdot K)$
thermal conductivity of insulation material	0.02 $W/(m \cdot K)$
insulation layer thickness	0.1 m

In practice, the thermal load, i.e., the heat injected into the ground through the boreholes in the soil borehole thermal energy storage systems is not constant, but a step thermal load. For example, if the heat is collected through solar collectors, the thermal load in the daytime varies with the solar radiation intensity, and the thermal load is only provided by the circulating fluid heated during daytime. As a simple case, it is assumed that the system is charged 12 hours with a thermal load of 80 W/m and another 12 hours with a thermal load of 40 W/m every day periodically. The method used to calculate temperature responses under step thermal load is the basic method to consider step heat transfer rate as presented in the research by Chen et al. [38].

Based on the case scenario described above, the borehole temperature responses were calculated using the new model proposed in this paper. Figure 14 gives the temperature response on the top of borehole under the three different ground surface boundary condition. It can be seen that under Neumann and Robin boundary condition, the temperatures on borehole top (24.3 °C and 22.8 °C respectively) are much larger than those under Dirichlet boundary condition (10.9 °C). The temperature differences just demonstrate the effects of insulation layer which remarkably reduced the heat loss through ground surface. In other words, in the application of borehole thermal energy storage systems where the borehole top is covered with insulation material, the traditional models which adopt a Dirichlet boundary condition on ground surface cannot give accurate temperature responses of borehole under the insulation cover.

Figure 15 shows the average temperature differences along the depth of the

borehole on borehole wall. Assuming the insulation cover gives perfect insulation, the temperature is the highest (18.8 °C). Considering the specific thermal resistance of the insulation cover, the temperature is 17.9 °C. In contrast, while adopting the Dirichlet boundary condition on ground surface, the average temperature is the lowest (17.1 °C). The temperature difference of a single borehole might be small, it would contribute to a great amount of thermal energy stored in the ground soil of borehole group, especially in the long time. Therefore, when designing the soil borehole thermal energy systems, using the traditional heat source models which employ a Dirichlet boundary condition would probably underestimate the heat storage capacity of the systems.

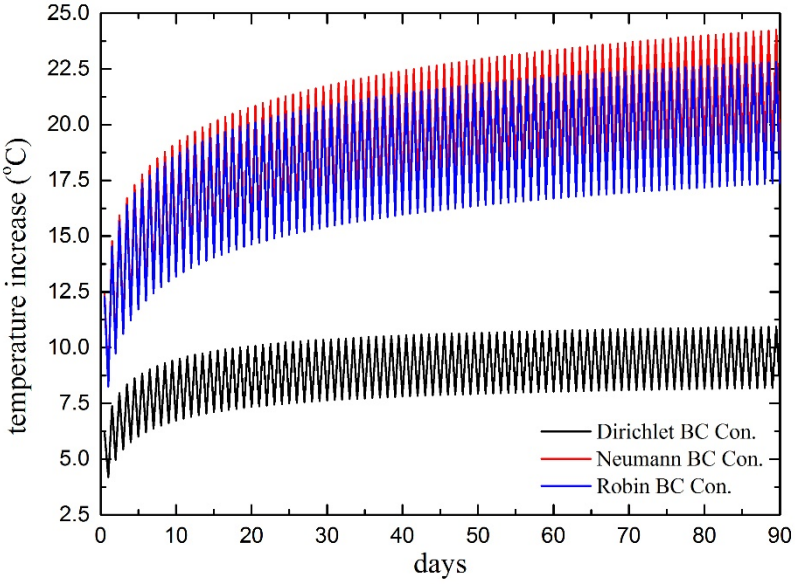

Figure 14 Temperature responses on the borehole top

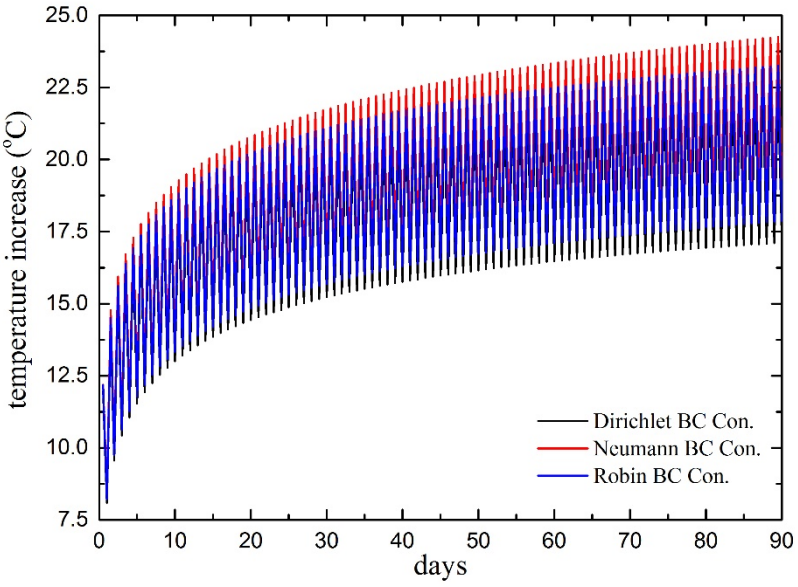

Figure 15 Average temperature responses on borehole wall

6. Conclusion

Most of the existing analytical models for vertical GHE employ either a constant temperature or changing ground surface temperature on ground surface as a Dirichlet boundary condition. However, a Robin boundary condition is closer to the real ground surface boundary condition. This paper successfully employed a new method, i.e., the integral transform method, to develop new analytical models for vertical GHE under three different types of ground surface boundary condition: the Dirichlet, Neumann, and Robin boundary condition. The solution equations under Robin boundary condition (Equations (36) and (37)) are flexible in giving the real ground surface boundary conditions.

The proposed heat source model was validated by comparing the results with the existing “solid” cylindrical heat source model. Using the new analytical models under the three different types of boundary conditions, the temperature and vertical heat flux around vertical GHE under the homogenous ground surface boundary condition of each type were calculated and analyzed. The purpose of only considering the homogeneous part of each boundary condition is to offer a theoretical and referential analysis of the influence of defining different ground surface boundary conditions on the heat transfer process of vertical GHE excluding the disturbance of the specific inhomogeneous part of each boundary condition, which may differ greatly in different places and in different applications.

It was found that generally, the influence of defining different types of ground surface boundary condition on the temperature profile of vertical GHE is limited in the dimensionless depth of 200. In this case, one obvious conclusion is that for vertical GHE with shorter depth, it is more important to defining the Robin ground surface boundary condition. Also, the selection of ground surface boundary condition should be seriously considered for different applications.

Under Robin boundary condition, the temperature profile is between the profiles of Dirichlet and Neumann boundary condition. When the convective heat transfer

coefficient is small, the profile would approach that of Neumann boundary condition. On the other hand, when it gets large, the profile would close that of Dirichlet boundary condition. For the ground surface has a convective heat transfer coefficient of 0.1, 0.5, or 2.5, the dimensionless temperature on ground surface would stabilize at approximately 0.4, 0.2, or 0.1 respectively.

Regarding the vertical heat flux, different definitions on ground surface boundary condition have no impact on the vertical heat flux at the bottom and middle depths of vertical GHE with a dimensionless depth of 200. The impact is limited in the upper part of vertical GHE. The larger the convective heat transfer coefficient, the larger the vertical heat flux through the ground surface. A common characteristic of vertical heat flux near two ends of vertical GHE is that it quickly diminishes with the increase of radius. Within the dimensionless radius of 10, the value of vertical heat flux decreases to only about 90% of that near borehole wall.

By defining a Robin ground surface boundary condition, the thermal impact, i.e., temperature and vertical heat flux, on the ground surface caused by the operation vertical GHE were firstly calculated and analyzed. The temperature would decrease with the increase of convective heat transfer coefficient, while the vertical heat flux has the opposite trend. Also, it seems that the vertical heat flux decreases much faster in radial direction compared with the temperature. Although the thermal impact near the ground surface caused by a single GHE might be minimal, the thermal impact of large borehole groups might be carefully checked for environmental concern.

Acknowledgements

This work was partially supported by the RGC General Research Fund (PolyU 152010/15E).

Reference

1. Sarbu, I. and C. Sebarchievici, *General review of ground-source heat pump systems for heating and cooling of buildings.* Energy and buildings, 2014. **70**: p. 441-454.
2. Yang, H., P. Cui, and Z. Fang, *Vertical-borehole ground-coupled heat pumps: A review of models and systems.* Applied Energy, 2010. **87**(1): p. 16-27.
3. Yuan, Y., et al., *Ground source heat pump system: A review of simulation in China.* Renewable and Sustainable Energy Reviews, 2012. **16**(9): p. 6814-6822.
4. Li, M. and A.C. Lai, *Review of analytical models for heat transfer by vertical ground heat exchangers (GHEs): A perspective of time and space scales.* Applied Energy, 2015. **151**: p. 178-191.
5. Fadejev, J., et al., *A review on energy piles design, sizing and modelling.* Energy, 2017.
6. Cui, Y., et al., *Techno-economic assessment of the horizontal geothermal heat pump systems: A comprehensive review.* Energy Conversion and Management, 2019. **191**: p. 208-236.
7. Dasare, R.R. and S.K. Saha, *Numerical study of horizontal ground heat exchanger for high energy demand applications.* Applied Thermal Engineering, 2015. **85**: p. 252-263.
8. Selamat, S., A. Miyara, and K. Kariya, *Numerical study of horizontal ground heat exchangers for design optimization.* Renewable energy, 2016. **95**: p. 561-573.
9. Go, G.-H., et al., *Optimum design of horizontal ground-coupled heat pump systems using spiral-coil-loop heat exchangers.* Applied energy, 2016. **162**: p. 330-345.
10. Li, C., et al., *Numerical simulation of horizontal spiral-coil ground source heat pump system: Sensitivity analysis and operation characteristics.* Applied Thermal Engineering, 2017. **110**: p. 424-435.
11. Wang, D., L. Lu, and P. Cui, *A new analytical solution for horizontal geothermal heat exchangers with vertical spiral coils.* International Journal of Heat and Mass Transfer, 2016. **100**: p. 111-120.
12. Jeon, J.-S., S.-R. Lee, and M.-J. Kim, *A modified mathematical model for spiral coil-type horizontal ground heat exchangers.* Energy, 2018. **152**: p. 732-743.
13. Han, C., et al., *Influence of local geological data on the performance of horizontal ground-coupled heat pump system integrated with building thermal loads.* Renewable energy, 2017. **113**: p. 1046-1055.
14. Fujii, H., et al., *Numerical modeling of slinky-coil horizontal ground heat exchangers.* Geothermics, 2012. **41**: p. 55-62.
15. Saadi, M.S. and R. Gomri, *Investigation of dynamic heat transfer process through coaxial heat exchangers in the ground.* International Journal of Hydrogen Energy, 2017. **42**(28): p. 18014-18027.
16. Demir, H., A. Koyun, and G. Temir, *Heat transfer of horizontal parallel pipe ground heat*

exchanger and experimental verification. Applied thermal engineering, 2009. **29**(2-3): p. 224-233.
17. Bortoloni, M., M. Bottarelli, and Y. Su, *A study on the effect of ground surface boundary conditions in modelling shallow ground heat exchangers.* Applied Thermal Engineering, 2017. **111**: p. 1371-1377.
18. Oosterkamp, A., T. Ytrehus, and S.T. Galtung, *Effect of the choice of boundary conditions on modelling ambient to soil heat transfer near a buried pipeline*. Applied Thermal Engineering, 2016. **100**: p. 367-377.
19. Kayaci, N. and H. Demir, *Numerical modelling of transient soil temperature distribution for horizontal ground heat exchanger of ground source heat pump*. Geothermics, 2018. **73**: p. 33-47.
20. Li, C., et al., *Influence of ground surface boundary conditions on horizontal ground source heat pump systems*. Applied Thermal Engineering, 2019. **152**: p. 160-168.
21. Bandos, T.V., et al., *Finite line-source model for borehole heat exchangers: effect of vertical temperature variations.* Geothermics, 2009. **38**(2): p. 263-270.
22. Bidarmaghz, A., et al., *The importance of surface air temperature fluctuations on long-term performance of vertical ground heat exchangers.* Geomechanics for Energy and the Environment, 2016. **6**: p. 35-44.
23. Rivera, J.A., P. Blum, and P. Bayer, *Ground energy balance for borehole heat exchangers: vertical fluxes, groundwater and storage.* Renewable energy, 2015. **83**: p. 1341-1351.
24. Zarrella, A. and P. Pasquier, *Effect of axial heat transfer and atmospheric conditions on the energy performance of GSHP systems: A simulation-based analysis*. Applied Thermal Engineering, 2015. **78**: p. 591-604.
25. Rivera, J.A., P. Blum, and P. Bayer, *Analytical simulation of groundwater flow and land surface effects on thermal plumes of borehole heat exchangers.* Applied energy, 2015. **146**: p. 421-433.
26. Rivera, J.A., P. Blum, and P. Bayer, *A finite line source model with Cauchy-type top boundary conditions for simulating near surface effects on borehole heat exchangers.* Energy, 2016. **98**: p. 50-63.
27. Rivera, J.A., P. Blum, and P. Bayer, *Influence of spatially variable ground heat flux on closed-loop geothermal systems: Line source model with nonhomogeneous Cauchy-type top boundary conditions.* Applied energy, 2016. **180**: p. 572-585.
28. Man, Y., et al., *A new model and analytical solutions for borehole and pile ground heat exchangers*. International Journal of Heat and Mass Transfer, 2010. **53**(13): p. 2593-2601.
29. Poularikas, A.D., *Transforms and applications handbook*. 2010: CRC press.
30. Korn, G.A. and T.M. Korn, *Mathematical handbook for scientists and engineers: definitions, theorems, and formulas for reference and review*. 2000: Courier Corporation.
31. LEUTENEGGER, M., *https://documents.epfl.ch/users/l/le/leuteneg/www/Author.html*
32. Valsa, J. and L. Brančik, *Approximate formulae for numerical inversion of Laplace transforms.* International Journal of Numerical Modelling: Electronic Networks, Devices and Fields, 1998. **11**(3): p. 153-166.
33. Baddour, N. and U. Chouinard, *Theory and operational rules for the discrete Hankel*

transform. JOSA A, 2015. **32**(4): p. 611-622.
34. Abate, J. and W. Whitt, *A unified framework for numerically inverting Laplace transforms.* INFORMS Journal on Computing, 2006. **18**(4): p. 408-421.
35. Villinger, H., *Solving cylindrical geothermal problems using the Gaver-Stehfest inverse Laplace transform.* Geophysics, 1985. **50**(10): p. 1581-1587.
36. Georgiev, A., A. Busso, and P. Roth, *Shallow borehole heat exchanger: Response test and charging–discharging test with solar collectors.* Renewable Energy, 2006. **31**(7): p. 971-985.
37. Başer, T. and J.S. McCartney, *Transient evaluation of a soil-borehole thermal energy storage system.* Renewable Energy, 2018.
38. Chen, Y., et al., *Thermal response factors for fast parameterized design and long-term performance simulation of vertical GCHP systems.* Renewable energy, 2019. **136**: p. 793-804.